Published in final edited form as:

Anal Chem. 2022 April 26; 94(16): 6139–6145. doi:10.1021/acs.analchem.1c05090.

Coupling stable isotope labelling and LC-TIMS-TOF MS/MS for *de novo* mosquito ovarian lipid studies

Lilian V. Tose[†], **Cesar E. Ramirez**[†], **Veronika Michalkova**[‖], **Marcela Nouzova**[§,‡], **Fernando G. Noriega**[‡], **Francisco Fernandez-Lima**[†,*]

[†]Department of Chemistry and Biochemistry, Biomolecular Sciences Institute, Florida International University, Miami, FL 33199, United States

[‖]Institute of Zoology SAS, Dúbravská cesta 9, 845 06 Bratislava, Slovak Republic

[§]Biology Center of the Academy of Sciences of the Czech Republic, Institute of Parasitology, 37005, Ceske Budejovice, Czech Republic

[‡]Department of Biological Sciences, Biomolecular Science Institute, Florida International University, Miami, FL, 33199

Abstract

There is a need to better understand the lipid metabolisms during the mosquito ovarian development. Lipids are the major source of energy supporting ovarian follicles development in mosquitoes. In this paper, we describe the complementary use of stable isotope labelling (SIL) and high-resolution mass spectrometry-based tools for the investigation of *de novo* triglycerides (TG) and diglycerides (DG) during the ovarian previtellogenic (PVG) stage (4 - 6 days post-eclosion) of female adult *Aedes aegypti*. Liquid chromatography coupled to high resolution trapped ion mobility spectrometry – parallel accumulation sequential fragmentation - mass spectrometry (LC-TIMS-PASEF TOF MS/MS) allowed the separation and quantification of non-labeled and $^{2}H/^{13}C$-labelled TG and DG species. Three SIL strategies were evaluated ($H_2O/^{2}H_2O$ with 50:50 and 95:5 mixtures, ^{13}C-sucrose, and ^{13}C-glucose). Results showed wide applicability with no signs of lipid ovarian impairment by SIL induced toxicity. The analytical workflow based on LC-TIMS-TOF MS/MS provided high confidence and high reproducibility for lipid DG and TG identification and SIL incorporation based on their separation by RT, CCS, and accurate *m/z*. In addition, the SIL fatty acid chain incorporation was evaluated using PASEF MS/MS. The $^{2}H/^{13}C$

[*]**Corresponding Author**: Francisco Fernandez-Lima – *Department of Chemistry and Biochemistry, Biomolecular Science Institute, Florida International University, Miami, Florida 33199, USA;* fernandf@fiu.edu.
Lilian V. Tose – *Department of Chemistry and Biochemistry, Florida International University, Miami, Florida 33199, United States.*
Cesar E. Ramirez – *Department of Chemistry and Biochemistry, Florida International University, Miami, Florida 33199, USA.*
Veronica Michalkova – *Institute of Zoology SAS, Dubravska Cesta 9, 84506 Bratislava, Slovakia; Department of Biology, Florida International University, Miami, FL 33199, USA.*
Marcela Nouzova – Department of Biology and Biomolecular Sciences Institute, Florida International University, Miami, FL 33199, USA.; Institute of Parasitology, Biology Centre CAS, Ceske Budejovice, Czech Republic.
Fernando G. Noriega – *Department of Biology and Biomolecular Sciences Institute, Florida International University, Miami, FL 33199, USA.*

Supporting Information

The Supporting Information is available free of charge at http://pubs.acs.org. Figures and Tables containing the lipid assigments, RT, CCS, Ko, MS/MS reporter ions, molecular ions forms, lipid distributions and SIL incorporation efficiency and enrichment. LC-TIMS-TOF MS raw files can be accessed via the FIU research Data Portal.

The authors declare no competing financial interest.

incorporation into the mosquito diet provided information on how TG lipids are consumed, stored, and recycled during the PVG stage of ovarian development.

Graphical Abstract

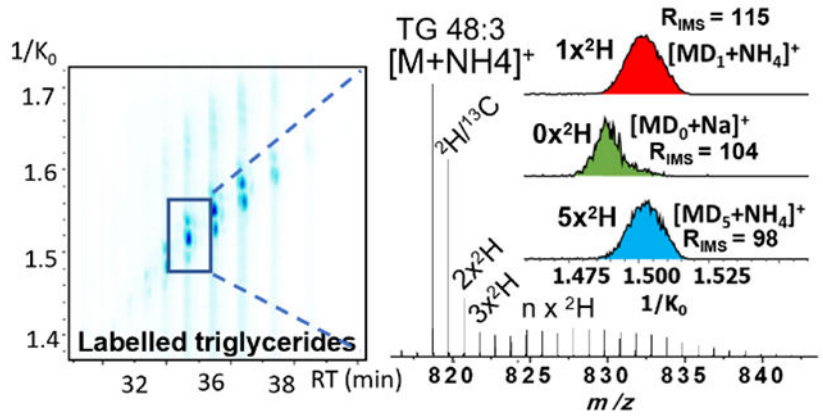

Introduction

For almost a hundred years, stable isotopes labelling (SIL) has been used to study lipid distribution, mobilization, and metabolism, as well as lipid synthesis dynamics.[1–5] Carbon (^{13}C) or hydrogen (^{2}H) SIL incorporation allows for the study of lipid metabolism without compositional changes that might affect organismal physiology.[6–13] $^{13}C/^{2}H$ are usually incorporated into precursors of acetyl-CoA units (e.g., deuterated water, ^{13}C-Glucose, or ^{13}C-acetate), leading to their integration into the fatty acids (FA). The higher abundance of these isotopes above the natural background is typically used as the based for their discrimination.[8] The number of $^{2}H/^{13}C$ incorporations into *de novo* synthesized lipids depends on the rate of flux through the fatty acid synthesis pathway.[8]

SIL incorporation can be critical during development of living systems due to the toxicity of some stable isotopes.[9] For example, studies have shown that ^{2}H from heavy water is lethal for living systems at 20% - 40% levels[14], and typical applications utilize below 10%.[9, 14] On the other hand, ^{13}C incorporations up to 70% in live organisms had no toxicity effects.[15]

Metabolic pathways are a fundamental expression of biological activity, and a priority for studies into the regulation of synthetic and biochemical processes in the mosquito life cycle.[16–20] Lipids are the most abundant source of energy and support essential biological processes in mosquitoes (e.g., growth, energy reserves, and reproductive capability).[21, 22] Several studies have successfully applied SIL to elucidate metabolic pathways for *de novo* synthesized lipids and their correlation with vital cellular processes.[8, 9, 11, 12]

The successful implementation of the SIL technique requires the removal of interferences from endogenous molecules, thus requiring the use of ultra-high resolution analytical tools.[7, 10, 23–25] In a recent study, a stable isotope labeled-sugar diet using deuterated water enabled the dynamic study of *de novo* diglycerides (DG) and triglycerides (TG) in mosquito ovaries using liquid chromatography (LC) in tandem with the high accuracy (< 0.3 ppm)

and ultra-high, mass resolution (over 1 M) of a 14.5 T Fourier Transform Ion Cyclotron Resonance Mass Spectrometer (14.5 T FT-ICR MS) equipped with hexapolar detection.[11] The lipid species were separated in the LC domain, while the ultra-high, mass resolution allowed for the separation of potential interferences at the nominal mass level (e.g., ^{2}H and ^{13}C A+1 ions). The SIL LC-FT-ICR MS workflow provided a benchmark for the study of *de novo* TG using SIL; however, this analytical platform is limited to few laboratories. There is a need for equivalent or better SIL workflows based on more accessible instrumentation platforms.

In the present work, we describe a complementary SIL and liquid chromatography coupled to high resolution trapped ion mobility spectrometry– parallel accumulation sequential fragmentation - mass spectrometry (LC-TIMS-PASEF -TOF MS/MS) workflow for the study of *de novo* DG and TG in female mosquito ovaries of *Aedes aegypti* during previtellogenic (PVG) stage (4 - 6 days post-eclosion) is described. Three sources of SIL for the mosquito diet were considered: $H_2O/^{2}H_2O$ (50:50 and 95:5) mixtures, ^{13}C-sucrose, and ^{13}C-glucose). In addition, to the superior analytical separation of *de novo* DGs and TGs provided by the RT and CCS, tandem MS/MS experiments allowed to trace SIL incorporation into the fatty acids. The $^{2}H/^{13}C$ stable isotope incorporation were measured as a function of the mosquito diet and time after eclosion and results showed differences at the individual *de novo* TG level.

EXPERIMENTAL SECTION

Materials and Reagents.

A Tuning Mix calibration standard from Agilent Technologies (Santa Clara, CA) was used. Sucrose-$^{13}C_{12}$, D-Glucose-$^{13}C_6$, and heavy water ($^{2}H_2O$) were purchased from Sigma-Aldrich (St. Louis, MO). A mixture of labelled lipid internal standards (EquiSsplash Lipidomix) from Avanti Polar Lipids (Alabaster, AL) was used.

Insects.

Aedes aegypti of the Rockefeller strain were raised in a room held at 28 °C and 80% humidity. After eclosion, adult mosquitoes were separated into six diet regimens: a) 20% Glucose/distilled water (DI); b) 20% Sucrose/DI; c) 20% 13C-Glucose/DI. d) 20% 13C-Sucrose/DI; e) 20% Sucrose with a $H_2O/^{2}H_2O$ (95:5, or 5% $^{2}H_2O$); and f) 20% Sucrose with a $H_2O/^{2}H_2O$ (50:50, or 50% 2H2O). The insects were fed daily by wetting a 1×1 inch cotton pad with the respective diet. A 20% sucrose/DI diet was considered as a biological control. Containers were loosely covered with a polyethylene wrap to prevent rapid evaporation of the feeding pad.

Dissection and extraction of lipids.

Female mosquito cohorts fed in six different diets were collected at two time points after adult eclosion: 4 and 6 days. Ovaries were dissected using a phosphate buffered saline solution. A total of 10 ovaries were collected per sample replicate, stored in 1.5 ml Eppendorf tubes, and kept frozen at −80 °C. Aliquots of 100 μL butanol/methanol, 3 μL

butylated hydroxytoluene and 10 μL of the labelled lipid internal standard mixture (10 ppm) were added to the Eppendorf tubes containing 10 ovaries.

The homogenization process was carried out for 10 seconds using 1.5 mL polypropylene pestles (Fisher Scientific, Pittsburgh, PA) and a handheld cordless motor. The pestles were then rinsed with 200 μL butanol/methanol, combining the rinse effluent with the homogenized solution. Next, Eppendorf tubes containing homogenates were sonicated at room temperature for 30 minutes and then centrifuged at 1,600 × *g* for 10 minutes. The supernatant was transferred into auto sampler vials with 300 μL silanized glass inserts (Thermo Fisher Scientific, Waltham, MA).

LC-TIMS-MS/MS analysis.

A Prominence LC-20 CE Ultra-Fast Liquid Chromatograph (Shimadzu, Japan) equipped with an Accucore C30 column (Thermo Fisher Scientific, Sunnyvale, CA), coupled to a commercial timsTOF (Bruker Daltonics Inc., Billerica, MA). The LC program consisted of a gradient separation between 30:40:30 and 10:5:85 acetonitrile (ACN), water (H_2O), and isopropanol (IPA). Mobile phase composition was changed as follows: sample injection at 0% B and hold for 1 min. From 1 to 5.6 min increase to 55% B and hold until 6.4 min. Increase to 65% B at 6.4 min and hold until 24 min. Increase to 88% B at 24 min until 40.8 min. Increase to 95% B until 48.1 min. After 48.1 min, decrease to 35% B and hold until 56 min. The last step, decrease to 0% B at 56 min and hold until 60 min. A 10 mM ammonium acetate and 0.1% formic acid was added. HPLC conditions were an injection volume of 5 μL, with a solvent rate of 0.25 mL/min, and 60 minutes total run. The LC program included an internal mobility and mass calibration section based on the Tuning Mix calibration standard.

Samples were ionized using an ESI source based on the Apollo II design (Bruker Daltonics Inc, Billerica, MA) in positive ion mode. Typical ESI operating conditions were 4500 V capillary voltage, 800 V end plate offset, 4.0 bar nebulizer pressure, 4.0 L/min dry gas, 250 °C dry heater and 200 μL/min injection flow. The timsTOF instrument was operated under parallel accumulation serial fragmentation (PASEF) for tandem MS/MS lipid FA assignment.[34] The LC-TIMS-MS/MS data was processed using a custom-building script in Data Analysis 5.2 software (Bruker Daltonics. MA). All spectra were mobility and *m/z* internally calibrated using the Tuning Mix calibration standard. Lipid abundances were calculated based on the LC retention time peak areas using a mobility and *m/z* extraction filter (<5 ppm tolerance).

Calibration curves were prepared by adding a known amount of lipid internal standard mixture and spiking with 10 μL of deuterated internal standard lipid mixture. The curve was built using seven calibration points ranging from 0.1 to 500 ng/mL with a constant 10 ng/mL of deuterated internal standard mixture. The PC, DG and TG lipids ID have been previously identified in these types of samples[11, 13] and the fatty acid chains were manually annotated based on the PASEF MS/MS patterns (tables S2, S4 and S6). The SIL labeling efficiency was calculated as the ratio of the area of the SIL containing isotopes (corrected by the effect of the potential A+1-A+4 interferences) to the area of the non-SIL containing isotopes. The SIL enrichment was calculated by fitting the experimental isotopic

profiles with a theoretical pattern. The theoretical pattern was determined by the probability of finding a labeled atom at any single site[35]. The values were calculated using biological triplicates for all diet conditions. Data are provided in Tables S1–S8.

RESULTS AND DISCUSSION

LC-TIMS-TOF MS/MS analysis of ovarian lipids.

The lipids extracted from mosquito ovaries were analyzed using LC-TIMS-PASEF TOF MS/MS. The list of lipid candidate assignments, from a non-labelled SIL diet is provided in Table S1, in good agreement with previous reports. [11, 13] The DGs and TGs were mostly detected in the $[M+NH_4]^+$ ion forms, while $[M+Na]^+$ ions were also observed at a lower abundance (Table S1). A total of 38 DG and TG species of lipids were successfully detected, distributed over a RT of 24 - 42 min and a 556 – 934 *m/z* range. In addition, the mobility values (CCS and $1/K_0$) are reported for all observed species (Table S1). The fatty acid distributions were determined based on the PASEF MS/MS experiments using the FA MS/MS reporter ions (Table S2, and S4).

In the case of SIL experiments, the chemical complexity significantly increased when compared to traditional lipid analyses (see Figure 1 and S1). For example, the effects of $^2H/^{13}C$ SIL on the RT, mobility and m/z are illustrated for TG 48:3, 48:2, 48:1 and 48:0 in Figure 1. The 48:0-48:3 TGs were separated by RT and mobility. Under the LC conditions utilized, no significant shift in RT was observed with the $^2H/^{13}C$ incorporations, in good agreement with previous reports.[11] Moreover, the mass distribution significantly changed with the $^2H/^{13}C$ incorporations. For example, at the RT =38 – 39 min, the mass projection corresponding to the ^2H SIL showed a significant increase in complexity with respect to non-labelled samples (Figure S1 c-d). In the case of non-labeled samples, the chemical complexity derives from the observation of different ion forms for each TG specie (TG 48:1/ TG 50:2 / TG 52:3) and from potential interferences from endogenous compounds. Moreover, the ^2H SIL samples carried all the ^2H incorporations (up to 20 units in the case shown in Figure S1). In the mobility dimension, while no separation was observed between ^2H SIL incorporations (e.g., $1/K_0 = 1.525$, $[M+NH_4]^+$ and, $1/K_0 = 1.528$ $[D_5M+NH_4]^+$, Figure S1), the different TG ion forms were mobility separated (e.g., $1/K_0 = 1.525$, $[M+NH_4]^+$ and $1/K_0 = 1.515$ $[M+Na]^+$, Figure S1). In addition to the DG and TG, some phosphatidylcholine (PC) species (PC 32:2/ 32:1/ 32:0) were identified in the protonated form (see Figure S2).

An advantage of complementary LC-TIMS-PASEF-TOF MS/MS experiments is that the MS signal of all TG and DG species can be filtered both by the RT and mobility, significantly reducing potential interferences of endogenous molecules. For example, molecular ions with *m/z* difference less than 4 mDa (e.g., TG 48:2 $1\times^2H$ and TG 48:3 $3\times^2H$) were separated by RT and mobility (mobility resolving powers up to 120 were observed). Due to the lower mass resolution of the TOF MS (typically 50k) compared to the FT-ICR MS (over 1M), the A+1-A+4 interferences were not resolved during $^2H/^{13}C$ SIL by the TOF MS analyzer. Nevertheless, for the purpose of comparing *de novo* synthesized vs teneral (carried from the larval stage), DG and TG reserves, the MS A+1-A+4 distributions could be corrected using as a reference the isotopic profile of the non-labeled samples (see inset of Figure 1e and 1f).

The DG and TG lipid species were separated based on the number of unsaturations in the LC domain (see Figure 2 b, d). The incorporation of a mobility separation, in addition to increasing the peak capacity and reducing the chemical noise, added certain orthogonality with respect to the LC separation (see Figure 2 a, c). As the size of the DG and TG increases, we observed an increase in the both retention times and CCS values for the $[M+NH4]^+$ ions. Closer inspection to the RT vs CCS and RT vs *m/z* plots showed that the slope for each DG and TG changed more dramatically in the RT vs CCS domain with the number of unsaturations as the DG and TG size increased in the RT vs *m/z* domain. These trends were also observed for $[M+Na]^+$ DG and TG ion forms (see Figures 2 and S3). Furthermore, inspection of the RT/equivalent carbon number (ECN) as function of the size, showed predictable trends: i) a decrease with the number of unsaturations and ii) constant value across with the same number of unsaturations for all TG considered (Figure S4).[35]

An increase in the CCS values was observed with the increase in the number of $^2H/^{13}C$ for all DGs and TGs. This CCS increase is expected due to the increase in the number of sub-atomic particles during SIL. The observed CCS values corresponded to the average of the positional isomers during the $^2H/^{13}C$ SIL of the DGs and TGs. Nevertheless, differences in mobility between the $^2H/^{13}C$ were observed. To estimate the position of the SIL (^2H or ^{13}C atoms), CID MS/MS experiments were performed on $10\times^2H$-labelled and $6\times^{13}C$-labelled TG 48:3 (Table S8 and Figure S5). Inspection of the $^2H/^{13}C$ SIL MS/MS showed that 2-3 positional isomers were observed based on the lengths and number of unsaturations. Further experiments using $^2H/^{13}C$ DG and TG standards could better assess capability of the mobility analysis to separate the positional isomers.

Influence of the $^2H/^{13}C$ SIL on the retention time, CCS and mass.

Differences in the mass accuracy (δ) were observed during $^2H/^{13}C$ SIL. The ^{13}C SIL do not introduce any mass interferences when respect to the non-labeled analysis and leaded to high mass accuracy measurements (δ < 1.5 ppm across triplicate injections).

The use of ^2H SIL results in the nominal mass overlap with naturally occurring ^{13}C atoms for the A+1-A+4 ions. These signals in the TOF MS analyzers are typically unresolved (see example in Figure 1 e, f). The change in the centroid position leads to a δ of up to 7 ppm (see Figure 3 B). Note that for $^2H_{5\text{-}20}$, this effect is no longer relevant due to the low contribution of ^{13}C atoms (δ < 2 ppm across triplicate injections).

Inspection of the relative standard deviation percentages (% RSD) across triplicate measurements showed high reproducibility in the RT and CCS measurements (<2%, Figure 3 c, d) across all identified DG and TG species for the three conditions studied (non-labelled, ^2H-Labelled, and ^{13}C-Labelled). In addition, a good agreement was observed between the measured $^{TIMS}CCS_{N2}$ and the reported $^{DT\text{-}IMS}CCS_{N2}$ (see Table S1)[26]. The CCS comparison revealed a Pearson correlation coefficient of r = 0.96887 for DGs and r = 0.99433 for TGs (Figure S6). In addition to the comparisons between candidate DG and TG species, similar results were obtained for the comparisons using a lipid standard mixture (Figure S7).

Identification and quantification of TGs and DGs from mosquito ovaries.

Aedes aegypti female mosquitoes can synthesize lipids *de novo* from sugar feeding.[11, 19, 22, 27–31] The $^{2}H/^{13}C$ SIL LC-TIMS-TOF MS experiments allowed to follow changes in the DG and TG lipid species in the ovaries during the previtellogenic (PVG) stage. The *de novo* synthesized TGs and DGs had the characteristic presence of $^{2}H/^{13}C$ in their elemental composition. The analysis of $^{2}H/^{13}C$ SIL incorporation dynamics allowed following individual lipid species. Visual differences (e.g., ovarian size and discoloration) were not observed regardless of the level of heavy water utilized.

Nevertheless, for the purpose of ^{2}H SIL tracing, $H_2O/^{2}H_2O$ mixtures with 5% of heavy water provided a DG and TG labelling efficiency (enrichment) of 5-20% (~1%) and 50-80% (up to 9%), respectively (Table S3). For example, ^{2}H SIL experiments of *de novo* synthesized TG 50:1 at day 6 showed 4 as a median number of hydrogens, 78% labelling efficiency and 7% enrichment using 5% heavy water sucrose diet (Figure 4 and Table S3). In a 50% heavy water sucrose diet, the TG 50:1 at day 6 showed 16 deuterium (as median number), 52% labelling efficiency and 35% enrichment. The ^{13}C SIL experiments showed a DG and TG labelling efficiency (enrichment) of 5-10% (~1%) and 10-30% (up to 15%), respectively (Table S5) with no phenotypic differences in the ovarian development.

The total TG lipid amount increased with the days after eclosion for all diets. Non-labelled diet and heavy water diets (5% and 50%) showed similar total amounts of TG lipids (Figure 5 and S8), suggesting no deuterium-induced toxicity. The incorporation of $^{2}H/^{13}C$ SIL into the diet at the levels proposed showed similar DG and TG lipid dynamics, (Figure 5, S8 and S9). Overall, TGs containing 44, 46, 48, 50, 52, 54 and 56 carbons were the most abundant (Figure 5 and S8), in good agreement with previous reports.[11, 13, 26] These experiments also provided information on DG species containing 30, 32, 34, and 36 carbons. The amount of DG species per ovary decreased with time and were detected at the picogram level (10^{3} times lower than the TG species).

Results from the $^{2}H/^{13}C$ SIL experiments showed that the SIL incorporation was observed for all TGs species, but with unique dynamics per an individual TG. When using a 5% and 50% heavy water sucrose diet, the ^{2}H incorporation into TGs increased over time. In the case of ^{13}C SIL, ^{13}C-Glucose showed lower amount of total lipids than the non-labelled diet and the ^{13}C-Sucrose diet (see example of TG 50:5-50:2 in Figure 5, S8 and S9). The differences in total TGs observed when using ^{13}C-Sucrose vs ^{13}C-Glucose were in good agreement with previous experiments.[11, 13, 21].

In addition to the DG and TG, some phosphatidylcholine (PC) species were observed in the protonated form (see Table S6 and S7). The PC species showed a low SIL enrichment (~1%), similar to those observed for the DG species. This difference in enrichment with respect to the TGs suggests a much slower turn over mechanism of SIL incorporation for PC and DGs. The SIL observed in the TGs can be directly correlated to precursors of acetyl-CoA units and is in good agreement with the standing theory of energy accumulation in the ovaries in the form of TGs. Closer inspection of the ^{2}H SIL experiments showed unique dynamics depending on the TG number of carbons and unsaturations (Figure 4). No specific trends were identified, and we believe is a consequence of the biological processes

in place and physiological activities. Nevertheless, these results are in good agreement with previous experiments where dynamic constant adjustments of ovarian TG stores were observed[19, 32, 33].

CONCLUSIONS

We introduced the use of $^{2}H/^{13}C$ SIL in combination with LC-TIMS-TOF MS/MS for the analysis of DG and TG lipid dynamics in the study of mosquito oogenesis. The incorporation of $^{2}H/^{13}C$ labels allowed to track *de novo* synthesized TG and DG lipid species. Traditional analytical challenges associated with the separation and identification were discussed, as well as the unique advantages of complementary LC, IMS and MS/MS to increase the peak capacity, reduce chemical noise and increase confidence during the assignment and quantification (e.g., correction for the A+1-A+4 naturally occurring ^{13}C interferences when using $^{2}H/^{13}C$ SIL).. Noteworthy is the high mass accuracy and low % RSD of the RT and CCS measurements. The usefulness of $^{2}H/^{13}C$ SIL LC-TIMS-TOF MS/MS to study the changes of TG lipid species in the ovaries during the previtellogenic (PVG) stage was established. The workflow allowed to effectively trace *de novo* synthesized TGs and DGs based on the characteristic presence of $^{2}H/^{13}C$ in their elemental composition. The technique was suitable to follow changes in individual lipid species over time. A total of 38 species of lipids were successfully $^{2}H/^{13}C$-labelled and characterized in the 550 - 940 *m/z* range with a mass accuracy lower than 3 ppm. LC-TIMS-TOF MS effectively differentiated species based on the number of unsaturations and incorporated SIL signal from different labels diet (heavy water and ^{13}C-Sucrose/^{13}C-Glucose), without interferences in the *de novo* synthesis and transfer processes into the ovary. Non-labeled diet, 5% and 50% heavy water sucrose diet resulted in similar amounts of total TG lipids; with no phenotypical differences in ovarian development (e.g., size and discoloration); that is, no evidence of deuterium-induced toxicity was observed. ^{13}C-Sucrose diet and non-labelled diet also revealed similar total amount of TG lipids. Moreover, SIL using ^{13}C-Glucose showed lower amount of lipids in good agreement with previous reports. [11, 13, 21]

Results showed that TG lipid dynamics behave independently for each TG species, evidenced by the SIL incorporation efficiency, enrichment, and total lipid amount. This observation suggests that molecular level characterization of TG dynamics is needed for a better understanding of diet and fitness during the ovarian follicle development in mosquitoes.

Supplementary Material

Refer to Web version on PubMed Central for supplementary material.

ACKNOWLEDGEMENTS

This work was supported by the NIH grant No. R21AI135469 to FFL and R01AI04554 to FGN.

REFERENCES

1. Qiu M; Hu AL; Huang YMM; Zhao Y; He Y; Xu JM; Lu ZJ Elucidating degradation mechanisms of florfenicol in soil by stable-isotope assisted nontarget screening. J Hazard Mater 2021, 403.

2. Hark TJ; Savas JN Using stable isotope labeling to advance our understanding of Alzheimer's disease etiology and pathology. J Neurochem 2021, 159, 318–329. [PubMed: 33434345]

3. Grey AC; Tang M; Zahraei A; Guo G; Demarais NJ Applications of stable isotopes in MALDI imaging: current approaches and an eye on the future. Anal Bioanal Chem 2021, 413 (10), 2637–2653. [PubMed: 33532914]

4. Zheng JJ; Shields EE; Snow KJ; Nelson DM; Olah TV; Reily MD; Robertson DG; Shipkova PA; Stryker SA; Xin BM; Drexler DM The utility of stable isotope labeled (SIL) analogues in the bioanalysis of endogenous compounds by LC-MS applied to the study of bile acids in a metabolomics assay. Anal Biochem 2016, 503, 71–78. [PubMed: 27033006]

5. Zhang Y; Gao B; Valdiviez L; Zhu C; Gallagher T; Whiteson K; Fiehn O Comparing Stable Isotope Enrichment by Gas Chromatography with Time-of-Flight, Quadrupole Time-of-Flight, and Quadrupole Mass Spectrometry. Anal Chem 2021, 93 (4), 2174–2182. [PubMed: 33434014]

6. Sturup S; Hansen HR; Gammelgaard B Application of enriched stable isotopes as tracers in biological systems: a critical review. Anal Bioanal Chem 2008, 390 (2), 541–554. [PubMed: 17917720]

7. Stokvis E; Rosing H; Beijnen JH Stable isotopically labeled internal standards in quantitative bioanalysis using liquid chromatography/mass spectrometry: necessity or not? Rapid Commun Mass Sp 2005, 19 (3), 401–407.

8. Brandsma J; Bailey AP; Koster G; Gould AP; Postle AD Stable isotope analysis of dynamic lipidomics. Bba-Mol Cell Biol L 2017, 1862 (8), 792–796.

9. Lehmann WD A Timeline of Stable Isotopes and Mass Spectrometry in the Life Sciences. Mass Spectrom Rev 2017, 36 (1), 58–85. [PubMed: 26919394]

10. Trotzmuller M; Triebl A; Ajsic A; Hartler J; Kofeler H; Regittnig W Determination of the Isotopic Enrichment of (13)C- and (2)H-Labeled Tracers of Glucose Using High-Resolution Mass Spectrometry: Application to Dual- and Triple-Tracer Studies. Anal Chem 2017, 89 (22), 12252–12260. [PubMed: 29087685]

11. Tose LV; Weisbrod CR; Michalkova V; Nouzova M; Noriega FG; Fernandez-Lima F Following de novo triglyceride dynamics in ovaries of Aedes aegypti during the previtellogenic stage. Sci Rep 2021, 11 (1), 9636. [PubMed: 33953286]

12. Godin JP; Fay LB; Hopfgartner G Liquid chromatography combined with mass Spectrometry for C-13 isotopic analysis in life science research. Mass Spectrom Rev 2007, 26 (6), 751–774. [PubMed: 17853432]

13. Castellanos A; Ramirez CE; Michalkova V; Nouzova M; Noriega FG; Francisco FL Three Dimensional Secondary Ion Mass Spectrometry Imaging (3D-SIMS) of Aedes aegypti ovarian follicles. J Anal At Spectrom 2019, 34 (5), 874–883. [PubMed: 31680712]

14. Katz JJ; Crespi HL Deuterated Organisms - Cultivation and Uses. Science 1966, 151 (3715), 1187-&. [PubMed: 5325694]

15. Thomson JF Physiological effects of D20 in mammals. Ann N Y Acad Sci 1960, 84, 736–44. [PubMed: 13776654]

16. Ryan RO; van der Horst DJ Lipid transport biochemistry and its role in energy production. Annu Rev Entomol 2000, 45, 233–260. [PubMed: 10761577]

17. Canavoso LE; Jouni ZE; Karnas KJ; Pennington JE; Wells MA Fat metabolism in insects. Annu Rev Nutr 2001, 21, 23–46. [PubMed: 11375428]

18. Ziegler R; Ibrahim MM Formation of lipid reserves in fat body and eggs of the yellow fever mosquito, Aedes aegypti. Journal of insect physiology 2001, 47 (6), 623–627. [PubMed: 11249951]

19. Ziegler R Lipid synthesis by ovaries and fat body of Aedes aegypti (Diptera: Culicidae). Eur J Entomol 1997, 94 (3), 385–391.

20. Zhou G; Flowers M; Friedrich K; Horton J; Pennington J; Wells MA Metabolic fate of [14C]-labeled meal protein amino acids in Aedes aegypti mosquitoes. Journal of insect physiology 2004, 50 (4), 337–49. [PubMed: 15081827]

21. Zhu J; Noriega FG The Role of Juvenile Hormone in Mosquito Development and Reproduction. Adv Insect Physiol 2016, 51, 93–113.

22. Zhou G; Pennington JE; Wells MA Utilization of pre-existing energy stores of female Aedes aegypti mosquitoes during the first gonotrophic cycle. Insect biochemistry and molecular biology 2004, 34 (9), 919–25. [PubMed: 15350611]

23. Fu T; Oetjen J; Chapelle M; Verdu A; Szesny M; Chaumot A; Degli-Esposti D; Geffard O; Clement Y; Salvador A; Ayciriex S In situ isobaric lipid mapping by MALDI-ion mobility separation-mass spectrometry imaging. J Mass Spectrom 2020, 55 (9), e4531. [PubMed: 32567158]

24. Tsugawa H; Cajka T; Kind T; Ma Y; Higgins B; Ikeda K; Kanazawa M; VanderGheynst J; Fiehn O; Arita M MS-DIAL: data-independent MS/MS deconvolution for comprehensive metabolome analysis. Nat Methods 2015, 12 (6), 523–6. [PubMed: 25938372]

25. Schmelzer K; Fahy E; Subramaniam S; Dennis EA The lipid maps initiative in lipidomics. Methods Enzymol 2007, 432, 171–83. [PubMed: 17954217]

26. Blazenovic I; Shen T; Mehta SS; Kind T; Ji J; Piparo M; Cacciola F; Mondello L; Fiehn O Increasing Compound Identification Rates in Untargeted Lipidomics Research with Liquid Chromatography Drift Time-Ion Mobility Mass Spectrometry. Anal Chem 2018, 90 (18), 10758–10764. [PubMed: 30096227]

27. Wang XL; Hou Y; Saha TT; Pei GF; Raikhel AS; Zou Z Hormone and receptor interplay in the regulation of mosquito lipid metabolism. P Natl Acad Sci USA 2017, 114 (13), E2709–E2718.

28. Sturmey RG; Reis A; Leese HJ; McEvoy TG Role of Fatty Acids in Energy Provision During Oocyte Maturation and Early Embryo Development. Reprod Domest Anim 2009, 44, 50–58. [PubMed: 19660080]

29. Noriega FG Nutritional regulation of JH synthesis: a mechanism to control reproductive maturation in mosquitoes? Insect biochemistry and molecular biology 2004, 34 (7), 687–93. [PubMed: 15242710]

30. Foster WA Mosquito sugar feeding and reproductive energetics. Annu Rev Entomol 1995, 40, 443–74. [PubMed: 7810991]

31. Briegel H Metabolic Relationship between Female Body Size, Reserves, and Fecundity of Aedes-Aegypti. J Insect Physiol 1990, 36 (3), 165–172.

32. Clifton ME; Noriega FG Nutrient limitation results in juvenile hormone-mediated resorption of previtellogenic ovarian follicles in mosquitoes. Journal of insect physiology 2011, 57 (9), 1274–81. [PubMed: 21708165]

33. Caroci AS; Li Y; Noriega FG Reduced juvenile hormone synthesis in mosquitoes with low teneral reserves reduces ovarian previtellogenic development in Aedes aegypti. J Exp Biol 2004, 207 (Pt 15), 2685–90. [PubMed: 15201301]

34. Jeanne Dit Fouque K; Fenandez-Lima F Recent advances in biological separations using trapped ion mobility spectrometry - mass spectrometry. Trends Anal Chem 2019, 116, 308–315.

35. Rampler E; El Abiead Y; Schoeny H; Rusz M; Hildebrand F; Fitz V; Koellenperger G Recurrent topics in mass spectrometry-based metabolomics and lipidomics - standardization, coverage, and throughput. Anal Chem 2021, 93, 519–545. [PubMed: 33249827]

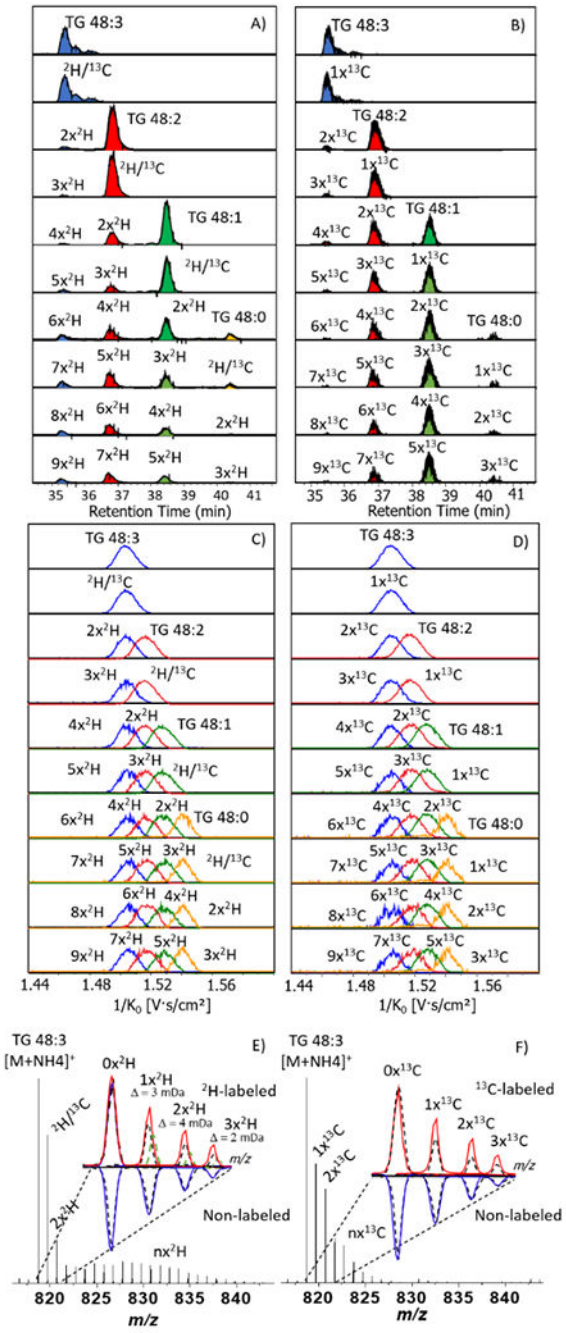

Figure 1.

Typical $[M+NH_4]^+$ extracted ion chromatograms and extracted mobilograms for the TG 48:3, 48:2, 48:1 and 48:0 from ^2H-labelled (A, C) and ^{13}C-labelled (B, D) from LC-TIMS-q-TOF MS/MS. Typical TOF MS spectra of TG 48:3 for ^2H-labelled (E) and ^{13}C-labelled (F). Amplified MS projections of ^2H and ^{13}C labelled isotope profiles (red) and non-labelled isotope profiles (blue). The theoretical isotope profiles are indicated as dash lines (^{13}C in black; ^2H in green).

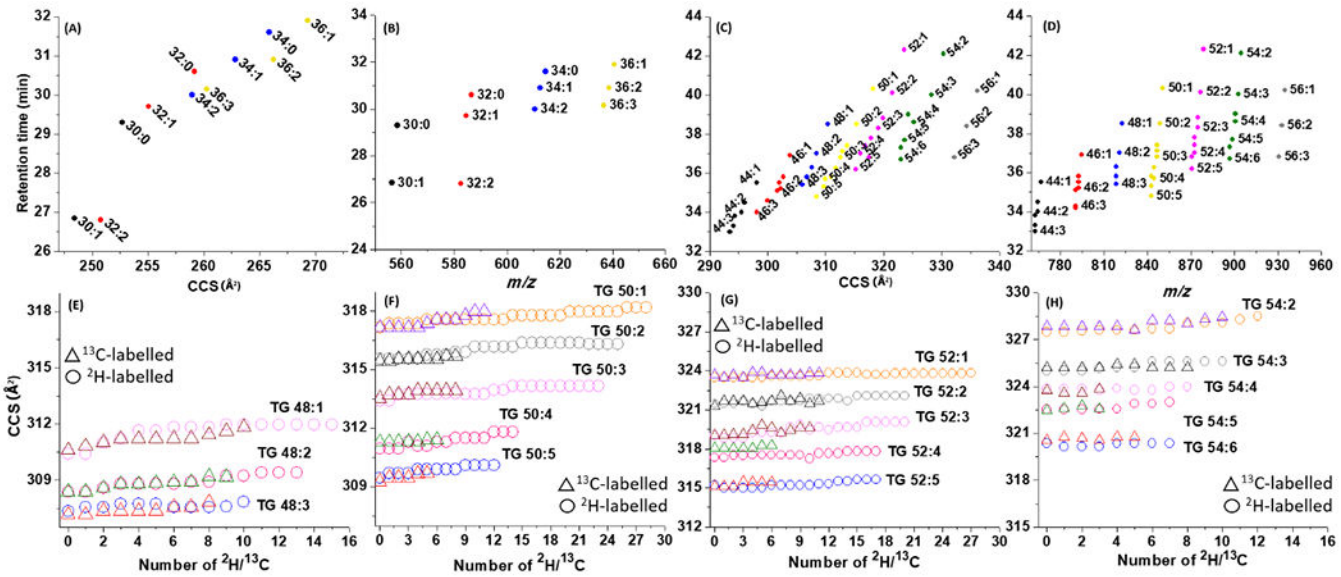

Figure 2.

RT vs CCS and RT vs *m/z* distributions for the $[M+NH_4]^+$ DG (A,B) and $[M+NH_4]^+$ TG (C, D) species. In (E-H), CCS dependence with the number of $^2H/^{13}C$ for $[M+NH_4]^+$ 48:1-3-54:2-6 TG species.

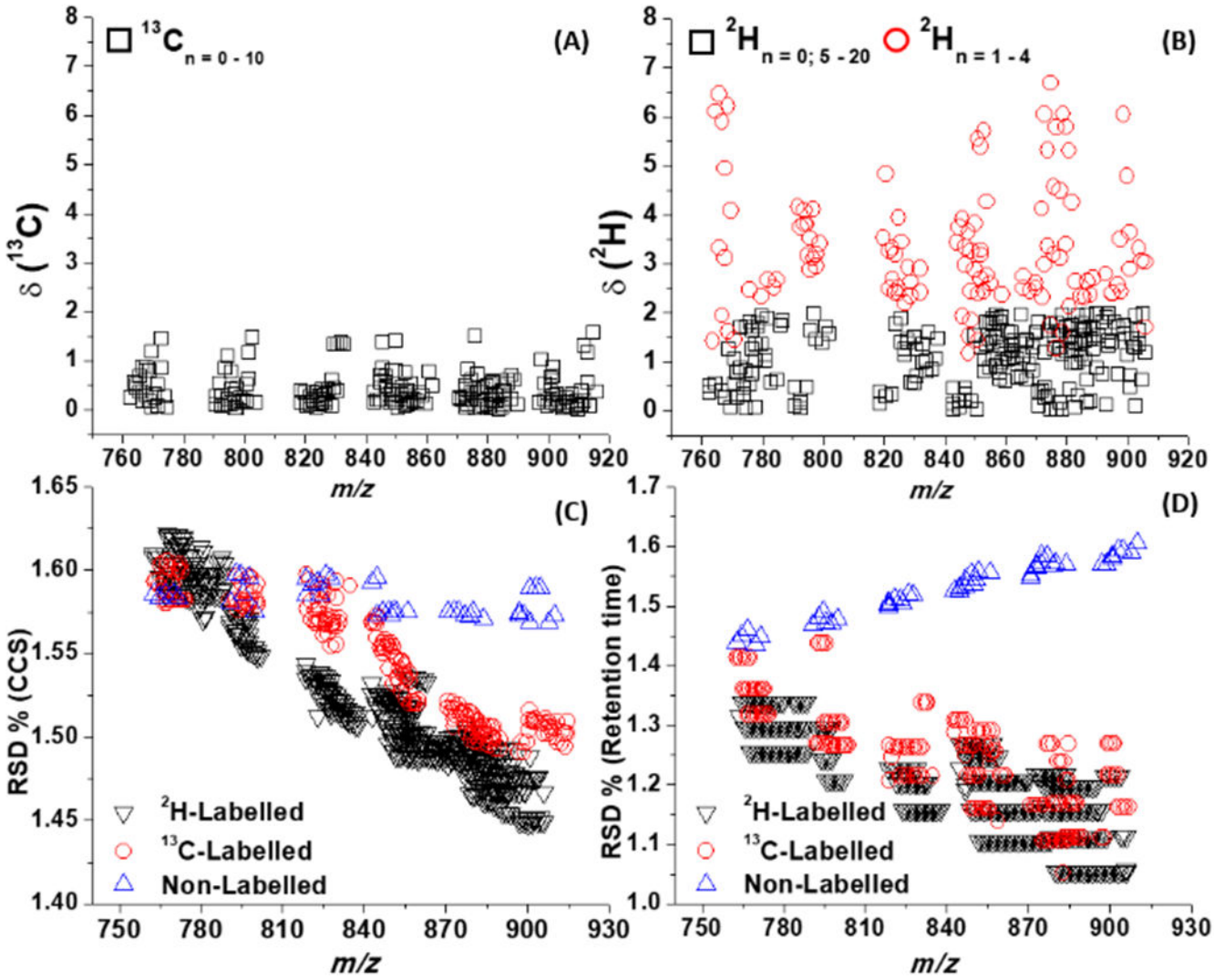

Figure 3.

Distribution of delta (δ) mass accuracy for TGs isotopes from $^{13}C_nTG$ (A) and $^{2}H_nTG$ (B). Distribution of relative standard deviation (RSD) of CCS (C) and Retention time (D) to $^{2}H/^{13}C$-labeled and non-labeled triglycerides.

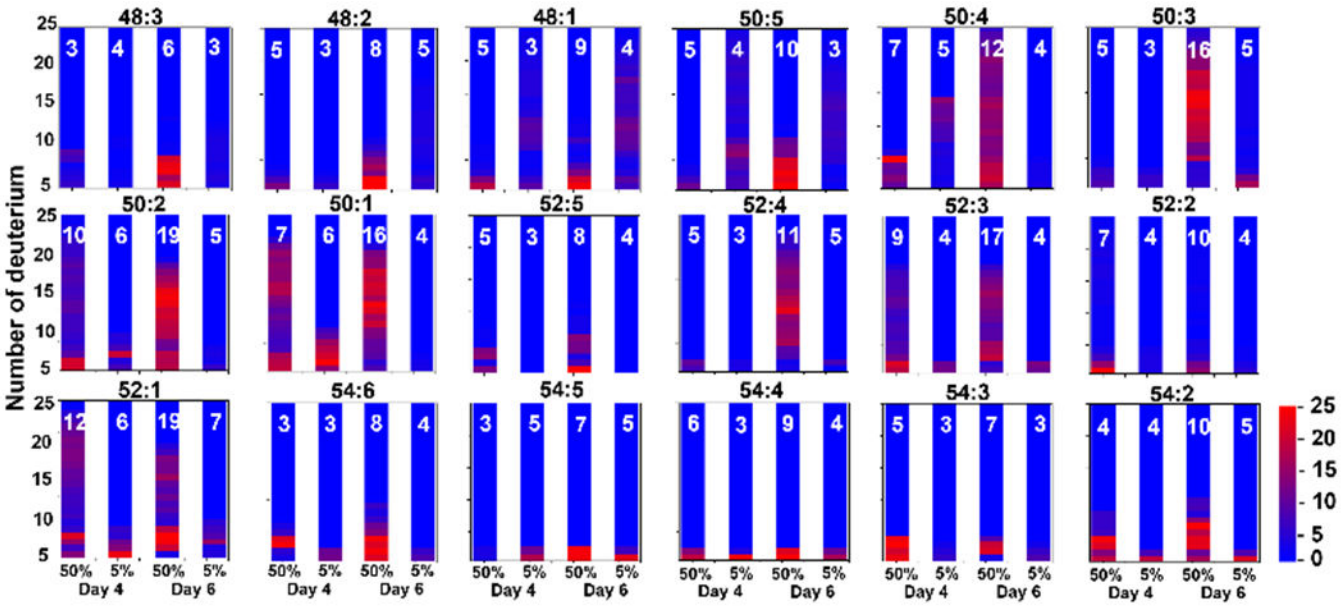

Figure 4.

Distribution of the number of deuteriums per TG species as a function of days and heavy water diet (50 % and 5 %) after eclosion (4-6 days). The median number of deuteriums is shown in the insets (white label). The color scale corresponds to the number of deuterated species relative to the TG 48:1 (d7) internal standard. *The scale intensity was normalized to TG 48:1 (d7) $[M+NH_4]^+$.

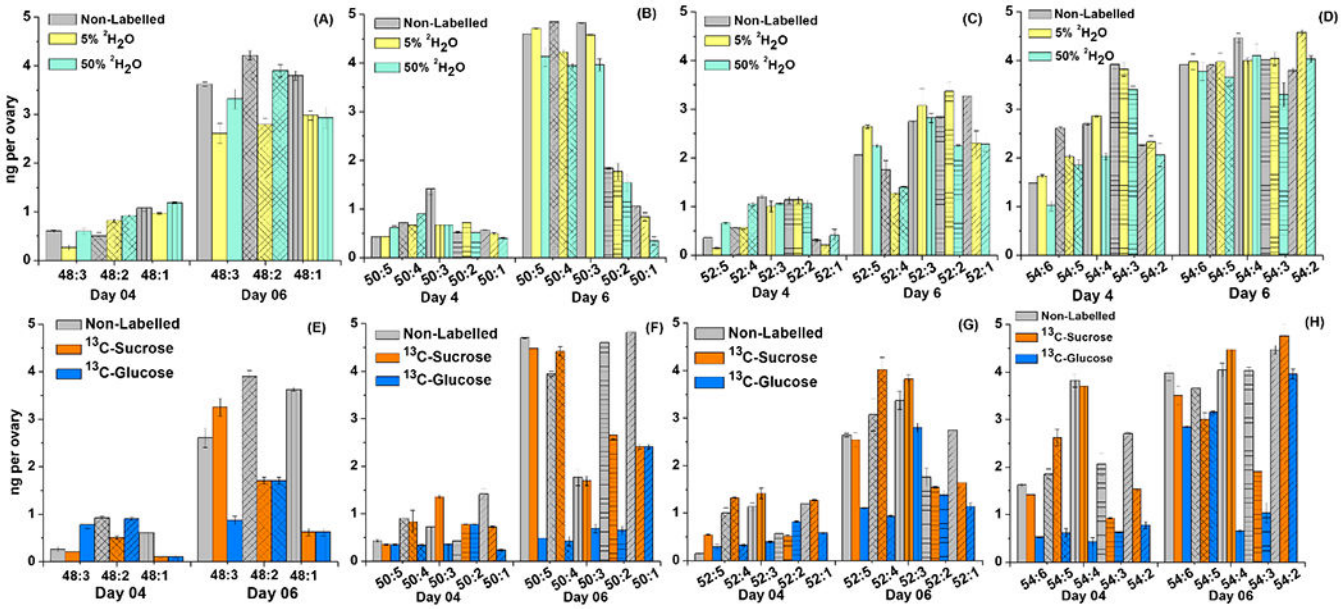

Figure 5.

Total lipid per ovary as a function of the TG species, diet and time. (A-D) 5% Heavy water *versus* 50% Heavy water with sucrose diet; (E-H) ^{13}C-Sucrose *versus* ^{13}C-Glucose. Error bars are means standard error (± SE) of the analysis of triplicates samples of 10 ovaries each.